Recieved:1 August, 2025 Accepted 9 October, 2025 https://doi.org/10.36582/ksj.2026.190773

AL-KUNOOZE SCIENTIFIC JOURNAL
ISSN: 2706-6231 E ,2706-6223 P
Vol.12 No.1 (2026)

Synthesis of Zinc Oxide Nanoparticles by Pulsed Laser Ablation in Liquid: Effect of Laser Pulse Energy on Prepared Particle Properties

Ali H. Ali, Jamal M. Rzaij*, Mustafa R. Al-Shaheen

Department of Physics, College of Science, University Of Anbar, Ramadi, Iraq

Corresponding author: sc.jam72al@uoanbar.edu.iq

Abstract

The present work explored a low-cost approach to synthesizing zinc oxide (ZnO) nanoparticles employing pulsed laser ablation in liquid (PLAL). The ablated material was pelletized into a disk with a diameter of 2 cm and annealed at 400 °C for one hour. NPs were prepared with a Q-switched Nd: YAG laser at 1064 nm wavelength and various energy levels (500, 600, and 700) mJ at a pulse count of 1000 pulses. The samples were initially examined by UV-Vis: for the latter, a power dependence (increasing laser power led to increased absorption in the 200–400 nm wavelength range) was found. The absorption peak was at about 370-380 nm. Furthermore, the Zeta potential increased with the higher laser power, indicating the superior stability of floating nanoparticles. Lastly, Flame Atomic Absorption Spectroscopy (FAAS) showed a power-dependent increase in the nanoparticles. For the UV-Vis, Zeta potential, and FAAS experiments, 700 mJ of power was the best condition. Hence, the selected samples were further analyzed for crystalline phase by X-ray diffraction (XRD), and atomic composition was determined by Energy Dispersive X-ray (EDX), size and shape were analyzed by Transmission Electron Microscope(TEM). The XRD diffraction data demonstrate various hexagonal phase crystalline structures for zinc (Zn), ZnO, and ZnO2. The diffraction peaks were exhibited at different 2θ positions and were calculated crystal sizes of (12.92–90.74) nm. EDX was used to verify that the nanoparticles have the targeted elemental stoichiometry. TEM examination confirmed the spherical shape of the particles with an average diameter of approximately 12 nm.

Keywords: Structural properties, ZnO NPs, pulsed laser, colloidal, Zeta potential

Introduction

Modern electronics are largely based on semiconductors, which have qualities between those of metals and insulators and whose conductivity is moderate and responsive to temperatures, light, or impurities. Their versatility, effectiveness, and resilience make them indispensable for the advancement of new responsive and energy-efficient technologies [1]. As one of the well-known metal oxide semiconductors, ZnO possesses a wide band gap, high electron mobility, and good chemical stability, which makes it an attractive material in the area of optoelectronics and sensor devices. The exemplary semiconducting properties are attributed to the presence of inherent defects and oxygen vacancies, which can be controlled by different synthetic and doping methods [2,3]. Nanoparticles are defined as particles between 1 and 100 nm that have unique physical, chemical, and biological characteristics at the nanoscale in contrast to their bulk [4,5]. This phenomenon is attributed to a number of factors, including increased ratio of surface area to volume, enhanced reactivity or stability in chemical processes, improved mechanical strength, and others [6,7]. Like CVD (chemical vapor deposition) and PVD (physical vapor deposition) have been used for the synthesis of Metal oxide-based nanomaterials[8]. Nanoprinting techniques, 3D nanoprinting [9], self-assembly [10], were other procedures, and the technique of nanoball milling was also used for the synthesis of nanoparticles[11,12]. Nevertheless, most of these approaches rely on toxic chemical treatments, leading to environmental issues, high expenses, and damage to living organisms. Consequently, there is a growing demand for safer, more efficient, and relatively easier methods. Pulsed laser ablation in liquids (PLA) is increasingly used as a method to synthesize nanocomposites using metallic sources under liquid environments [13]. The majority of previous work utilised a single laser energy source during nanoparticle synthesis [14]. The study presented here broadens the knowledge by analyzing the influence of multiple energy levels. Some work has been done in restricting to the energy spectrum or particle size alone [15]. It has been reported in the literature that laser energy plays an important role in determining the size, crystallinity, and surface charge of synthesized nanostructured ZnO particles,

which are some critical parameters to define their stability and functional performances [16].

This work underlines that considering the absorption behavior is a convenient alternative rather than previous reports that have mainly concentrated on estimating the bandgap from UV-Vis spectroscopy results. The major objective of this work is to fabricate high-quality ZnO NPs using a reliable method via PLAL with an enhancement in the applications similar to solar energy, water treatment, and biomedical. This sequential approach improves the synthesis and also provides a platform to optimize other semiconductor oxides. With larger surface areas and stability, these ZnO nanoparticles are promising in the applications of advanced photocatalytic coating and flexible optoelectronic devices. Furthermore, intrinsic biocompatibility offers advantages to targeted drug delivery systems [17]. Prepared ZnO nanoparticles via pulsed laser Ablation in Liquid (PLAL) at three various energies of the laser: 500 mJ, 600 mJ, and 700 mJ, with a fixed number of pulses being computed as 1000.

Experimental procedures and characterization

Five grams of the high-purity (99.9%) zinc oxide (ZnO) powder (Research Nanomaterials, Inc., USA) was fabricated as a ZnO target pellet. Pressure by a hydraulic press of 300 bar was applied to get the maximum height of the sample per unit volume and to remove the vacuum air from the prepared pellet with two dimensions, i.e., diameter: 2 cm and thickness: 5 mm, and kept it for 24 h. The sample was transferred to an oven at 400°C for one hour and kept there to anneal and dry, after which it was allowed to cool down to room temperature. After preparing the target (compressed sample) of ZnO, it was irradiated by a Q-switched Nd: YAG laser at a wavelength of 1064 nm with 1000 pulses and different pulse energies of 500, 600, and 700 mJ and a repetition rate of 4 Hz. It is worth considering that the sample was inserted into 10 ml ion-free distilled water, considering the dimensions of a recipient in which CD was placed, and so that the column of water above the disc did not exceed 5 mm, whereas the distance from the probe holder to the laser diode was equal to 12 cm. 10 ml of colloidal liquid was collected.

The UV-Vis absorption spectra of the ZnO nanoparticles were recorded with a UV-Vis spectrophotometer (model 1911DB, INOVIALAB, China) in the wavelength

range of 190–1100 nm. To determine the stability of ZnO nanoparticles in colloidal suspension, zeta potential was determined by a NanoBrook ZetaPlus analyzer (USA). Metals and minerals were analysed using Flame atomic absorption spectroscopy (FAAS) in samples. This is a Japanese-made knife. Company name: Shimadzu. Model: AA-7000. The morphology of ZnO NPs was determined by X-ray diffraction (XRD) analysis using a Shimadzu instrument with model number XD-6000. Elemental composition was analyzed by an energy-dispersive X-ray (EDX) spectrometer (Shimadzu Model: EDX-8000, Japan). The detailed morphologies at the nanoscale level were examined by a Titan 80-300 high-resolution transmission electron microscope.

Results and discussion

UV-Vis absorbance analysis

UV-Vis spectroscopy is one of the best and simplest methods used for spectrophotometry analysis, and can be applied even to a broad spectrum of compounds. It works by observing the interaction of electromagnetic radiation with matter at particular wavelengths [18]. The absorption spectra of ZnONP solutions in the range 200-800 nm are shown in Figure 1. Photons with high energy irradiate zinc oxide, resulting in the excitation of an electron from the valence to the conduction bands and thus more absorbed substances. For the 500 mJ energy model, a conspicuous peak can be seen at around 370 nm that is consistent with earlier reports [19,20]**.** Beyond which the absorbance decreases slowly as the wavelength increases [21]. The spectrum for the 600 mJ energy model is much like that of the 500 mJ, probably because equilibrium between evaporation and particle production has been reached, keeping the concentration constant [22].

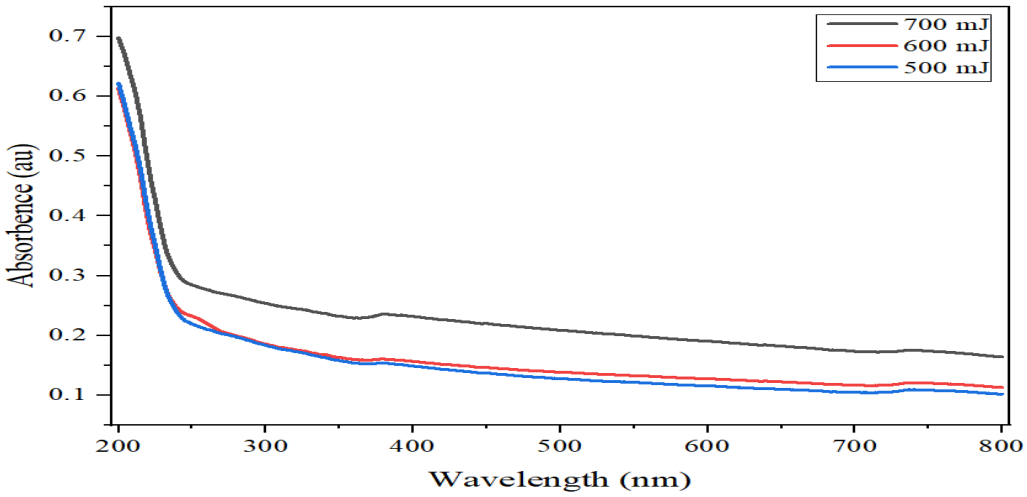

Figure (1): UV-Vis absorption spectra of ZnO nanoparticles synthesized at 1000 laser pulses and varying laser pulse energies (500, 600, and 700 mJ).

The 700 mJ sample, having higher energy, would show that it is no longer in balance. This leads to a higher evaporation rate and particle generation. The absorption increases with increasing power of the laser, possibly due to higher concentrations of ZnO-NPs. An increase in the laser power leads to smaller NPs. Smaller particles have more surface area relative to their volume. This reduces their friction with the surrounding medium and enhances absorption [23]. The maximum absorption occurs at 380 nm in the UV region; this result corresponds well with previous studies. [19,20].

Zeta potential results

Zeta potential is a key property of particles suspended in liquids, macromolecules, and material surfaces. Knowing about zeta potential can speed up the process of creating experimental formulations and indicate how stable they will be over time [24] [25]. Table 1 lists the zeta potential results of the zinc oxide colloids prepared at various pulse energies. The increasing laser pulse energy significantly increased the zeta potential, which is the same conclusion as that of Lotina et al. [26].

Table (1): Zeta potential results of ZnO at various Laser energy pulses

Pulse energy (mJ)	Zeta Potential (mV)
500	–30.93
600	–38.27
700	–47.30

Compared to previous zeta potential data that determine the electrical stability of nanoparticles, presented in Table 2, the prepared ZnO nanoparticles reveal good stability (Zeta potential between –30 and –47 mV), indicating a more repulsive force and higher stability, and reducing the possibility of agglomeration or aggregation [27].

Table (2): Electrical Stability Ranges of Nanoparticles [24]

Zeta Potential (mV)	Colloidal stability behavior
from 0 to ±5	Rapid coagulation or flocculation
from ±10 to ±30	Incipient instability
from ±30 to ±40	Moderate stability
from ± 40 to ±60	Good stability
more than ±61	Excellent stability

The zeta potential distribution curves for ZnO that were synthesised using 700,600, and 500 mJ pulse energies are shown in Figs (2a-c). The graphs reveal a percentage of zeta potential values within the negative region around –31 and –48 mV. A large negative potential implies the presence of repulsion between particles, which enhances suspension stabilization by preventing the agglomeration or aggregation. [28].

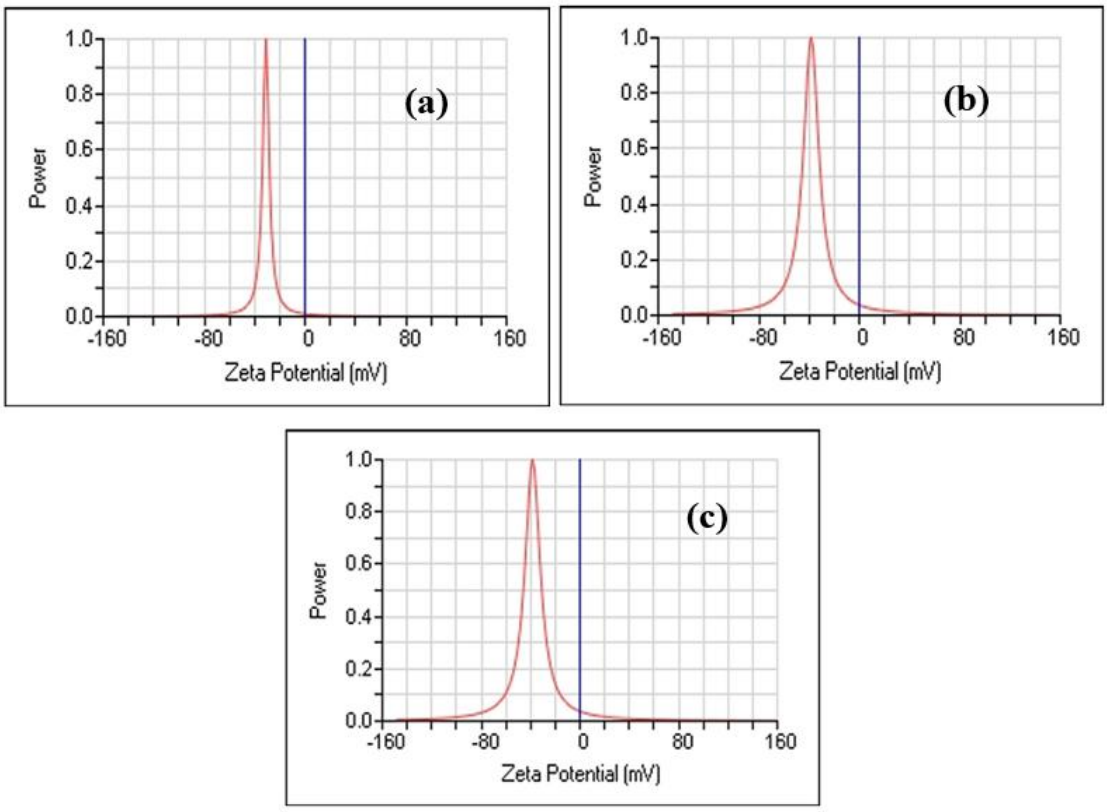

Figure (2): Zeta Potential of ZnO nanoparticles at Laser pulse energy of (a) 500 mJ, (b) 600 mJ, and (c) 700 mJ

The tight distribution around these values indicates uniform surface charge characteristics among particles, reinforcing the system's stability. According to these values, the three samples exhibit chemical and physical stability, with little likelihood of particle aggregation or loss of homogeneity in the short term.

Flame atomic absorption spectroscopy (FAAS)

The FAAS is widely used for the analysis of metals and metalloids in samples [29]. The pulsed laser irradiation induces the excitation of ZnO and creates zinc in measurable forms, allowing for the measurement of zinc concentration by methods such as FAAS [30]. The zinc contents for three mJ laser energy models (500, 600, and 700) are plotted in Table 3; at the value of 500 mJ is the zinc concentration of 4.10 (ppm). Meanwhile, the concentration of Zn at 600 mJ increased to 4.20 ppm. At 700 mJ, the maximum concentration of ZnO NPs (4.60 ppm) was obtained. The results demonstrated that the zinc content in the liquid tended to

increase at high laser pulse energy, which means higher efficiency of ablation. Higher energy in the laser pulse results in more energy delivered to the surface of the target per pulse, which then further contributes to ejecting material. This results in a better nanoparticle yield and a higher saturation of the surrounding solution [31].

Table (3): Zinc concentrations as a function of laser pulse energy

Pulse energy (mJ)	Zn (ppm)
500	4. 10
600	4. 20
700	4. 60

X-Ray diffraction analysis

It should be noted that X-ray diffraction (XRD) is a non-destructive and preferential method for studying the atomic structure of materials [32]. XRD was used to identify the hexagonal phase of the synthesized sample from Figure 3 and Table 4, where the multiple peaks are related to Zn, ZnO, and zinc peroxide (ZnO_2). All diffraction peaks were found at certain 2θ values, and the d-spacing Miller indices (hkl), i.e., (111), (200), (002), (102), (110), (103), and higher ones like (222) and even damaging one which is possibly a defective peak of ZnO crystal lattice [33]. Based on the JCPDS reference cards (01-078-1124, 01-075-1526, and 00-001-1238), the sample is mainly composed of a hexagonal wurtzite structure, which can be ascribed to ZnO. The existence of ZnOα was also proved by the identification peaks corresponding to (111), (200), and (222) planes, whereas elemental Zn was determined at 2θ = 36.82° for the (002) plane as per card number 00-001-1238 [34]. The crystallite sizes were obtained using the Scherrer equation (1) [35,36].

$$D = \frac{k\lambda}{\beta cos\theta}$$

(1),

where D is crystallite size, k is the Scherrer constant (often assumed to be 0.9), λ is the X-ray wavelength (1.54 nm), β is the FWHM of diffraction peak, and θ stands for Bragg angle, which indicates a broad range of D from 12.92 up to 90.74 nm. The (102) peak, which was located at 2θ = 48.18°, provided the narrowest full-width at half maximum (FWHM = 0.0959), and therefore, the highest calculated crystallite size θc (90.74 nm). Then, the FWHM of (222) plane at 2θ =

66.31° exhibited a larger width of 0.734, which corresponded to a smaller crystallite size of 12.92 nm (possibly due to more internal strain or structural defects) [37]. This Diffraction pattern confirms the good crystallinity of the sample with sharp, well-defined peak positions. The formation of ZnO_2 and Zn appears to be unexpected, such as by use of the particular laser ablation conditions (PLAL). Rapid and local heating and cooling by high-energy laser pulses can be achieved, resulting in partial oxidization, which may promote the coexistence of various zinc-based phases, as has also been reported elsewhere [38]. These results indicate that we have indeed synthesized ZnO nanostructures, predominantly in the hexagonal wurtzite phase, along with smaller amounts of Zn and ZnO_2. There are also differences in the crystallite size on different planes, indicating their dependence on the growth direction (local conditions) of these nanocrystals [39]. Crystallite size, which varies between 12.92 nm and 90.74 nm, is predicted to significantly affect material properties: smaller crystallites have greater surface reactivity due to more strain, whereas larger crystals are more crystalline with fewer defects, directly affecting optical, catalytic, and electronic properties [40].

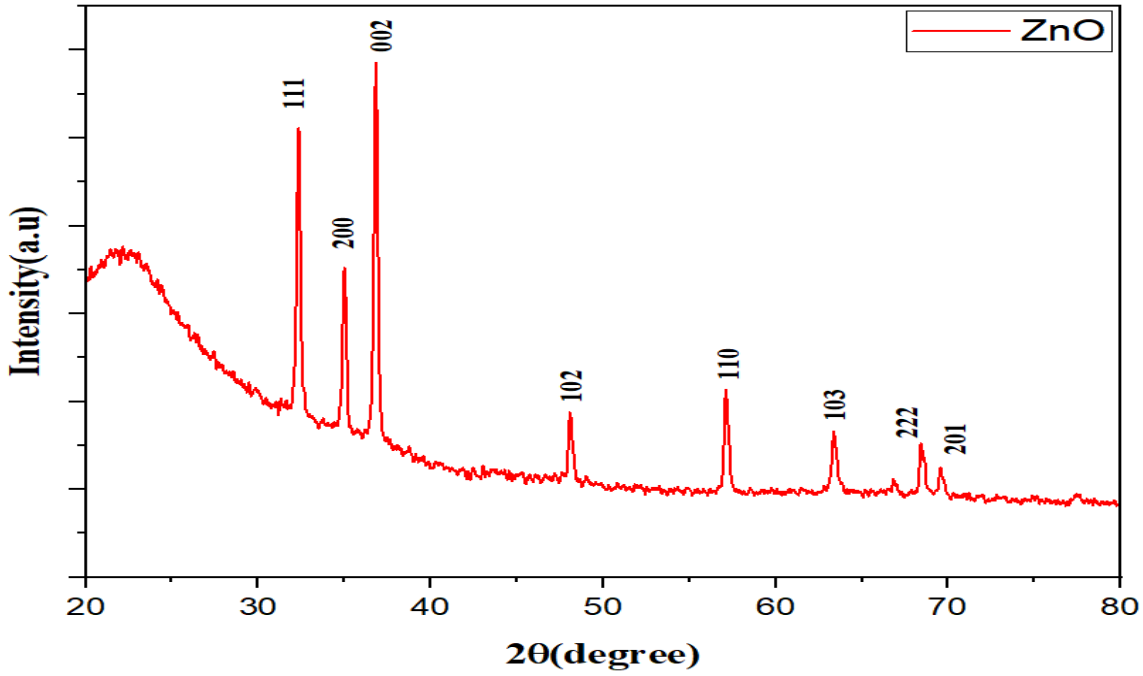

Figure (3) X-ray diffractogram of ZnO prepared with 700 mJ

Table (4): XRD analysis results of ZnO nanoparticles

2θ (deg.)	FWHM (deg.)	(hkl)	Crystallite size (nm)	Crystal system	Chemical formula	Card No.
32.32	0.3659	(111)	22.6	Hexagonal	ZnO_2	01-078-1124
35.07	0.5119	(200)	16.27	Hexagonal	ZnO_2	01-078-1124
36.82	0.3989	(002)	20.98	Hexagonal	Zn	00-001-1238
48.18	0.0959	(102)	90.74	Hexagonal	ZnO	01-075-1526
57.19	0.655	(110)	13.81	Hexagonal	ZnO	01-075-1526
63.56	2.4416	(103)	21.16	Hexagonal	ZnO	01-075-1526
66.31	0.734	(222)	12.92	Hexagonal	ZnO_2	01-078-1124
69.49	0.2047	(201)	47.23	Hexagonal	ZnO	01-075-1526

Energy dispersive X-ray (EDX) results

Elemental analysis by energy-dispersive X-ray (EDX) is another of the many analytical methods used to find elements in a given sample. The EDX spectrum of the zinc oxide nanoparticles produced by laser ablation is shown in Fig. 4. EDX measurements proved that the particle elements of interest are present as expected. The spectrum obviously shows peaks for two elements, Zn and O, patterns indicate that pure ZnO NPs were synthesized. Table 5 presents the additional peaks, which can be indexed to silicon (Si) originating from the silicon wafer substrate. The EDX analysis shows that the atomic percentage is 69.68% for Zn and 30.32% for O in the sample. These findings are in agreement with other reports [41].

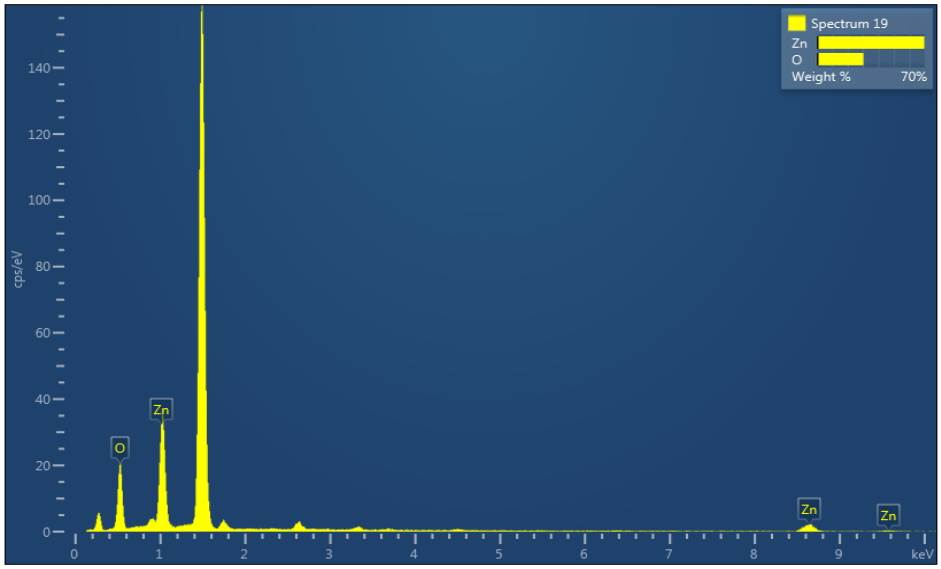

Figure (4): EDX spectrum of ZnO nanoparticles

Table 5: EDX elemental spectrum of ZnO nanoparticles

Element	Line Type	Wt. %	Atomic %
O	K series	30.32	64.00
Zn	L series	69.68	36.00
Total:		100	100

2.1 TEM analysis

Transmission Electron Microscopy (TEM) is well known for the high-resolution imaging of materials at the nanoscale level. TEM The TEM images provide important information about the morphology, crystallinity, and structural integrity of the nanoparticles [42]. It was observed from Figure 5 that Zinc oxide (ZnO) nanoparticles were generally well-defined in a circular shape and mostly nearly spherical.

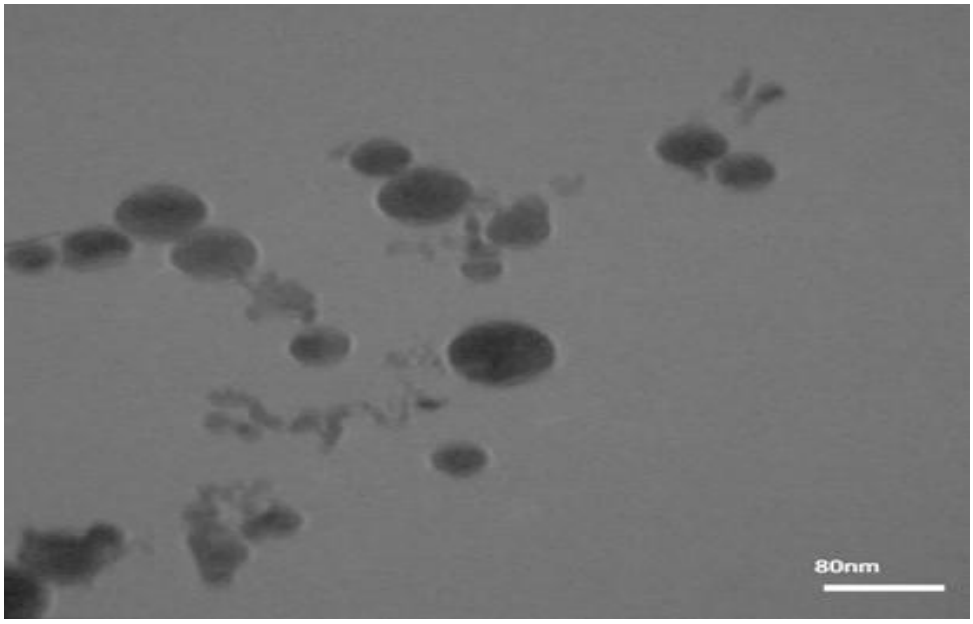

Figure (5): TEM image of ZnO

The particle size distribution analysis showed a clear dominance of smaller nanoparticles, with most being below 15 nm in diameter, as shown in Figure 6. Although most particles are Microscopic, with a few larger ones up to 42 nm, the smallest measure 2 nm. The median size is 8 nm, and the standard deviation is 11 nm; the average

particle size is 12 nm, indicating moderate size variation. Non-uniform energy distribution during laser ablation could cause this wide size range. Such features are common in nanoparticles produced by pulsed laser ablation in liquid (PLAL), where different particle populations can result from rapid nucleation and growth processes [43].

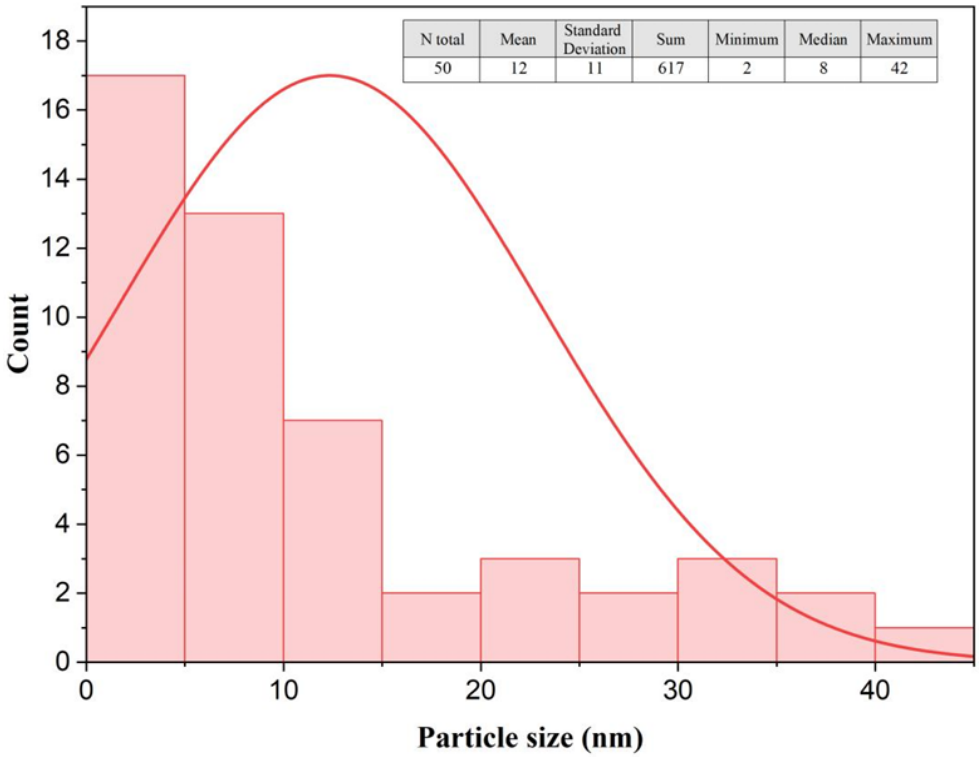

Figure (6): Particle size distribution of ZnO nanoparticles based on TEM analysis

3 Conclusions and Recommendations

ZnO nanoparticles were successfully synthesized through pulsed laser ablation in liquid using laser pulse energies of 500, 600, and 700 mJ. The optical absorption in the UV spectrum was enhanced by increasing the laser pulse energy, suggesting the formation of nanoparticles effectively. The crystalline nature of the ZnO nanoparticle being high was identified by X-ray diffraction (XRD) technique and found to be 12.92 nm to 90.74 nm in size range. Energy dispersive X-ray spectroscopy (EDX) was performed to determine the elemental composition, which revealed that Zn and O are present in these nanoparticles as expected for ZnO nanoparticles. TEM revealed predominantly spherical-shaped nanoparticles in the size range of 2-42 nm, which are consistent with

that of the crystallite size as estimated. The result suggests that high pulse energy during pulsed laser ablation enhances the quality, stability, and concentration of NPs for various ZnO NP applications.

It is suggested that future research is focused on changing other laser parameters, e.g., pulse duration, wavelength, and repetition rate, to enhance the distribution profile and properties of the nanoparticles. Extended studies on the performance, application, and functionality of ZnO NPs in photocatalytic/solar energy conversion and the biomedical field would add a great advantage for the practical utilization of these materials with a broader applicatory scope. Therefore, optimization of the synthesis procedure with control over particle size and stability is a prerequisite for large-scale production. Future studies may also investigate the long-term stability of NPs in a variety of liquid media and under various conditions. Integration of pulsed laser ablation with other surface modification techniques may improve the surface morphology of nanoparticles for specific applications, such as drug delivery and environmental remediation. A study comparing PLAL with other NPs producing methods could highlight differences in terms of purity, size precision, and environmental consideration.

Conflict of Interest: Authors declare there is no conflict of interest.

Reference

[1] Evstigneev M. *Introduction to semiconductor physics and devices*. Springer, 2022.

[2] Ali IM, Rzaij JM, Abbas QA, Ibrahim IM, Alatta HJ. Structural, Optical and Sensing Behavior of Neodymium-Doped Vanadium Pentoxide Thin Films. Iranian Journal of Science and Technology, Transactions A: Science. 2018; 42 (4):2375–86.

[3] He H. Metal oxide semiconductors and conductors. In: *Solution processed metal oxide thin films for electronic applications*. Elsevier, 2020:7–30.

[4] Tawfeeq HA, Rzaij JM. Effect of Thickness on the Structural and Optical Properties of Cadmium Oxide Thin Films Deposited by Thermal Vacuum Evaporation Technique. In: *Recent Trends and Advances in Artificial Intelligence and Internet of Things*.

Springer International Publishing, 2024:582–91.

[5] Rzaij JM, Abbas QA, Khalaf AM. Investigating the structural, topographical, morphological and optical effects of AgO on sprayed SnO2 thin films. Bulletin of Materials Science. 2023; 46 (4):200.

[6] Radwan HA, Marei JM, Khalefa AA, Rzaij JM. ZnO/PSi nanoparticles thin film for NO2 sensing application prepared by pulsed laser deposition. Indian Journal of Physics. 2024; 98 (2):455–67.

[7] Fan Z, Huang X, Tan C, Zhang H. Thin metal nanostructures: synthesis, properties and applications. Chem Sci. 2015; 6 (1):95–111.

[8] Adeoye AE, Adeaga OA, Ukoba K. Chemical Vapour Deposition (CVD) and Physical Vapour Deposition (PVD) techniques: Advances in thin film solar cells. Nigerian Journal of Technology. 2024; 43 (3):479–89.

[9] Zhang N, Wang Z, Zhao Z, *et al.* 3D printing of micro-nano devices and their applications. Microsyst Nanoeng. 2025; 11 (1):35.

[10] Borah R, Ag KR, Minja AC, Verbruggen SW. A review on self-assembly of colloidal nanoparticles into clusters, patterns, and films: emerging synthesis techniques and applications. Small Methods. 2023; 7 (6):2201536.

[11] Tawfeeq HA, Rzaij JM. The effect of Nb2O5 and pdo nanostructures coating on the structural and morphological properties of CdO thin films. In: *4TH INTERNATIONAL CONFERENCE ON PURE SCIENCES: ICPS2023*. Baghdad, Iraq, 2024:050011.

[12] Palos CMM, Mariño-Gámez AE, Acosta-González G-E, *et al.* Large-scale production of ZnO nanoparticles by high energy ball milling. Physica B Condens Matter. 2023; 656:414776.

[13] Mahdi MM, Salim ET, Obaid AS. Au@ Nb2O5 core/porous-shell nanoparticles: synthesis and characterization at different laser pulse. Mater Today Commun. 2025:112719.

[14] Glob MK, Hussain SA, Al-Mayalee KH. Preparation and Characterization of Titanium Dioxide Nanoparticles by Laser Ablation in Liquid. Iraqi Journal of Applied Physics. 2024; 20 (2A):163–8.

[15] Acosta-Humánez MF, Magon CJ, Montes-Vides L, Jiménez J, Almanza O. Structural, Magnetic, Optical and Photocatalytic Properties of Co-Doped ZnO Nanocrystals. Int J Mol Sci. 2025; 26 (5):2117.

[16] Singh A, Vihinen J, Frankberg E, Hyvärinen L, Honkanen M, Levänen E. Pulsed laser ablation-induced green synthesis of TiO 2 nanoparticles and application of novel small angle X-ray scattering technique for nanoparticle size and size distribution analysis. Nanoscale Res Lett. 2016; 11:1–9.

[17] Chen M, Wang Z, Li K, Wang X, Wei L. Elastic and stretchable functional fibers: a review of materials, fabrication methods, and applications. Advanced Fiber Materials. 2021; 3:1–13.

[18] Rzaij JM, Ibraheam AS, Abass AM. Cobalt Effect on the Growth of Cadmium Oxide Nanostructure Prepared by Spray Pyrolysis Technique. Baghdad Science Journal. 2021; 18 (2):0401.

[19] Florica C, Costas A, Preda N, *et al.* Core-shell nanowire arrays based on ZnO and CuxO for water stable photocatalysts. Sci Rep. 2019; 9 (1):17268.

[20] Khajuria AK, Kandwal A, Sharma RK, Bachheti RK, Worku LA, Bachheti A. In vitro antioxidant and antibacterial activities of biogenic synthesized zinc oxide nanoparticles using leaf extract of Mallotus philippinensis Mull. Arg. Sci Rep. 2025; 15 (1):6541.

[21] Khashan KS, Sulaiman GM, Abdulameer FA, *et al.* Antibacterial activity of TiO2 nanoparticles prepared by one-step laser ablation in liquid. Applied Sciences. 2021; 11 (10):4623.

[22] Filho HJI, dos Santos Salazar RF, da Rosa Capri M, Neto ÂC, de Alcântara MAK, de Castro Peixoto AL. State-of-the-Art and Trends in Atomic Absorption Spectrometry. Atomic Absorption Spectroscopy. 2011:13.

[23] Attallah AH, Abdulwahid FS, Ali YA, Haider AJ. Effect of liquid and laser parameters on fabrication of nanoparticles via pulsed laser ablation in liquid with their applications: a review. Plasmonics. 2023; 18 (4):1307–23.

[24] Mohammadi-Jam S, Waters KE, Greenwood RW. A review of zeta

potential measurements using electroacoustics. Adv Colloid Interface Sci. 2022; 309:102778.

[25] Albukhaty S, Al-Bayati L, Al-Karagoly H, Al-Musawi S. Preparation and characterization of titanium dioxide nanoparticles and in vitro investigation of their cytotoxicity and antibacterial activity against Staphylococcus aureus and Escherichia coli. Anim Biotechnol. 2022; 33 (5):864–70.

[26] Serrano-Lotina A, Portela R, Baeza P, Alcolea-Rodríguez V, Villarroel M, Ávila P. Zeta potential as a tool for functional materials development. Catal Today. 2023; 423:113862.

[27] Vakurov A, Drummond-Brydson R, Ugwumsinachi O, Nelson A. Significance of particle size and charge capacity in TiO2 nanoparticle-lipid interactions. J Colloid Interface Sci. 2016; 473:75–83.

[28] Dai H, Han T, Cui J, *et al.* Stability, aggregation, and sedimentation behaviors of typical nano metal oxide particles in aqueous environment. J Environ Manage. 2022; 316:115217.

[29] Ipeaiyeda AR, Ayoade AR. Flame atomic absorption spectrometric determination of heavy metals in aqueous solution and surface water preceded by co-precipitation procedure with copper (II) 8-hydroxyquinoline. Appl Water Sci. 2017; 7:4449–59.

[30] Kapukıran F, Kartoğlu B, Ebrar Karlıdağ N, Bakırdere S. Zinc Oxide Nanomaterial-Based Dispersive Solid Phase Extraction for the Trace Determination of Gold in Flash Gold Plating Solution Samples using Flame Atomic Absorption Spectrophotometry. ChemistrySelect. 2023; 8 (27):e202302384.

[31] Aguirre MA, Selva EJ, Hidalgo M, Canals A. Dispersive liquid–liquid microextraction for metals enrichment: A useful strategy for improving sensitivity of laser-induced breakdown spectroscopy in liquid samples analysis. Talanta. 2015; 131:348–53.

[32] Ali A, Chiang YW, Santos RM. X-ray diffraction techniques for mineral characterization: A review for engineers of the fundamentals, applications, and research directions. Minerals. 2022; 12 (2):205.

[33] Awan SU, Hasanain SK, Rashid J, *et al.* Structural, optical, electronic and magnetic properties of multiphase ZnO/Zn (OH) 2/ZnO2 nanocomposites and hexagonal prism shaped ZnO nanoparticles synthesized by pulse laser ablation in Heptanes. Mater Chem Phys. 2018; 211:510–21.

[34] Hessien M, Da'na E, Kawther AL, Khalaf MM. Nano ZnO (hexagonal wurtzite) of different shapes under various conditions: Fabrication and characterization. Mater Res Express. 2019; 6 (8):085057.

[35] KHALEFA AA, MAREI JM, RADWAN HA, RZAIJ JM. In2O3-CuO NANO-FLAKES PREPARED BY SPRAY PYROLYSIS FOR GAS SENSING APPLICATION. Dig J Nanomater Biostruct. 2021; 16 (1):197–204.

[36] Shawki OS, Rzaij JM. Effect of Fe2O3 upper layer on structural, morphological, and photoluminescence characteristics of TiO2 thin film prepared by chemical spray pyrolysis. In: *1st Diyala International Conference for Pure and Applied Science (ICPAS2021)*. Iraq: AIP Conference Proceedings, 2023:020009.

[37] Ismail MA, Taha KK, Modwi A, Khezami L. ZnO nanoparticles: Surface and X-ray profile analysis. J Ovonic Res. 2018; 14 (5):381–93.

[38] Anandan M, Dinesh S, Krishnakumar N, Balamurugan K. Tuning the crystalline size of template free hexagonal ZnO nanoparticles via precipitation synthesis towards enhanced photocatalytic performance. Journal of Materials Science: Materials in Electronics. 2017; 28:2574–85.

[39] Mohammada A, Al-Jafa HA, Ahmeda HS, Mohammedb M, Khodairc Z. Structural and morphological studies of ZnO nanostructures. Journal of Ovonic Research. 2022; 18 (3):443–52.

[40] Ibraheam AS, Rzaij JM, Arshad MKMd. Influence of Magnesium Content on the Structural, Optical, and Electrical Properties of Cu2(Zn1-xMgx)SnS4 Nanostructured Quaternary Thin Film Synthesized Using the Sol–Gel Method. J Electron Mater. 2023; 52 (1):414–21.

[41] Khattak U, Jan S, Ullah R, *et al.* Green synthesis and physical characterization of zinc oxide nanoparticles (ZnO NPs) derived from the methanol extract of Euphorbia dracunculoides

Lam.(Euphorbiaceae) with enhanced biosafe applications. Green Processing and Synthesis. 2024; 13 (1):20240119.

[42] Tang CY, Yang Z. Transmission electron microscopy (TEM). In: *Membrane characterization*. Elsevier, 2017:145–59.

[43] Mat Isa SZ, Zainon R, Tamal M. State of the art in gold nanoparticle synthesisation via pulsed laser ablation in liquid and its characterisation for molecular imaging: a review. Materials. 2022; 15 (3):875.

تخليق جسيمات أكسيد الزنك النانوية بواسطة الاستئصال بالليزر النبضي في السائل: تأثير طاقة نبضة الليزر على خصائص الجسيمات المحضرة

علي حسين علي، جمال مال الله رزيج، مصطفى رياض الشاهين

الخلاصة

بحثت هذه الدراسة في طريقة فعالة من حيث التكلفة لتخليق جسيمات نانوية من أكسيد الزنك (ZnO) باستخدام الاستئصال بالليزر النبضي في السائل (PLAL). تم ضغط المادة المستخرجة في أسطوانة بقطر 2 سم وتم تسخينها عند 400 درجة مئوية لمدة ساعة واحدة. تم تخليق الجسيمات النانوية باستخدام ليزر Nd:YAG متحول Q يعمل عند طول موجي 1064 نانومتر ومستويات طاقة مختلفة (500 و600 و700) مللي جول مع عدد نبضات 1000 نبضة. أولاً، تم تحليل العينات باستخدام التحليل الطيفي فوق البنفسجي المرئي (UV-Vis)، والذي أظهر أن زيادة طاقة الليزر أدت إلى زيادة مقابلة في الامتصاص ضمن نطاق الطول الموجي 200-400 نانومتر. كانت هناك ذروة امتصاص حول 370-380 نانومتر. أيضًا، زاد جهد زيتا مع زيادة طاقة الليزر، مما يشير إلى استقرار أفضل للجسيمات النانوية في المعلق. وأخيرًا، أشار مطياف الامتصاص الذري باللهب (FAAS) إلى أن تركيز الجسيمات النانوية يزداد مع استخدام طاقة الليزر. وقد تم الحصول على أفضل النتائج في تحليلات مطياف الأشعة فوق البنفسجية المرئية (UV-Vis) وجهد زيتا ومطياف الامتصاص الذري باللهب (FAAS) عند 700 مللي جول. لذلك، تم اختيار هذه العينات لمزيد من التوصيف باستخدام حيود الأشعة السينية (XRD) وتحليل الأشعة السينية المشتتة للطاقة (EDX) ومجهر الإلكترون النافذ (TEM). تشير نتائج حيود XRD إلى وجود هياكل بلورية متعددة في الطور السداسي تتوافق مع الزنك (Zn) وأكسيد الزنك (ZnO) وبيروكسيد الزنك (ZnO_2). ظهرت قمم الحيود عند قيم θ2 مميزة مع أحجام بلورية محسوبة تتراوح من (12.92 إلى 90.74) نانومتر. وأكد تحليل EDX أن الجسيمات النانوية الناتجة تمتلك البنية العنصرية المتوقعة. وأظهر تحليل المجهر الإلكتروني النافذ أن الجسيمات لها شكل دائري محدد جيدًا، ومتوسط حجم الجسيمات 12 نانومتر.

الكلمات المفتاحية: الخصائص الهيكلية، جسيمات نانوية من أكسيد الزنك، ليزر نبضي، غرواني، جهد زيتا